Uniqueness and wavelength optimization in continuous-wave multispectral diffuse optical tomography

Alper Corlu, Turgut Durduran, and Regine Choe

Department of Physics and Astronomy, University of Pennsylvania, Philadelphia, Pennsylvania 19104

Martin Schweiger, Elizabeth M. C. Hillman, and Simon R. Arridge

Department of Computer Science, University College London, Gower Street, London WC1E 6BT, UK

Arjun G. Yodh

Department of Physics and Astronomy, University of Pennsylvania, Philadelphia, Pennsylvania 19104

We derive conditions for the unique and simultaneous recovery of chromophore concentrations and scattering coefficients in multispectral continuous-wave diffuse optical tomography. These conditions depend strongly on measurement wavelengths. We introduce and demonstrate a general methodology for choosing those wavelengths, which yields superior separation of scattering from absorption and superior separation of one chromophore from another. Application of these concepts should significantly improve the fidelity of continuous-wave diffuse near-infrared optical tomography in tissues. © 2003 Optical Society of America

OCIS codes: 170.3010, 170.6960, 170.5280, 100.3190.

Diffuse optical tomography (DOT) has emerged as an important means to obtain physiologically relevant tissue parameters such as blood oxygen saturation (Y_T) and total hemoglobin concentration (THC).[1,2] Typically, near-infrared light is directed through tissue, and measurements of the transmitted light are made on the tissue boundary. Data acquisition can be accomplished with time-domain, frequency-domain, and CW methods. The CW method is technically the simplest scheme and potentially offers greater parallelism at lower cost. However, the inverse problem associated with CW DOT does not have unique solutions[3,4]; multiple sets of optical parameters can yield identical data for cw measurements.

In this Letter we describe a spectral approach for inversion of CW data that reduces the parameter cross-talk problem that arises from nonuniqueness, and we present a method for choosing optimal measurement wavelengths. The method is based on two aspects of the nonuniqueness problem: unique separation of absorption and scattering and minimization of cross talk between absorbing chromophores.

Our approach makes two assumptions. First, the wavelength-dependent tissue absorption is $\mu_a(\lambda) = \sum_i \epsilon_i(\lambda) c_i$, where c_i is the concentration and $\epsilon_i(\lambda)$ is the extinction coefficient of the ith chromophore at wavelength λ. Second, the wavelength-dependent tissue reduced-scattering coefficient is assumed to take on a simplified Mie-scattering form, $\mu_s'(\lambda) = a\lambda^{-b}$, where a and b are related to the size, the index of refraction, and the concentration of scatterers in the tissue as well as the index of refraction of the surrounding medium.[5,6] In the spectral model unknown parameters μ_a and μ_s' are replaced with unknown chromophore concentrations c_i and scatterer parameters a and b; reconstruction is performed with multispectral data simultaneously.[7,8] This scheme differs from conventional DOT,[2,9] wherein absorption and scattering are reconstructed separately at each wavelength and then combined to obtain chromophore concentrations; the number of unknowns increases with each additional wavelength in conventional DOT.

We recast uniqueness conditions for the spectral model starting with the photon diffusion equation for the light fluence rate $\Phi(\omega)$ in the frequency domain, i.e.,

$$-\nabla \cdot D\nabla\Phi(\omega) + \left(\mu_a + \frac{i\omega}{v}\right)\Phi(\omega) = q_o(\omega). \qquad (1)$$

Here ω is the source modulation frequency, v is the speed of light in the medium, $q_o(\omega)$ is an isotropic source that is assumed to be nonzero in a small layer of width $z_0 \sim 1/\mu_s'$ from the boundary, and D is the photon diffusion coefficient approximately[10,11] given by $1/(3\mu_s')$.

Following Arridge and Lionheart,[3] we make the substitutions $\gamma^2 = D$ and $\Psi = \gamma\Phi$, so Eq. (1) can be rewritten as $-\nabla^2\Psi(\omega) + \eta(\omega)\Psi(\omega) = q_o(\omega)/\gamma$, where $\eta = \eta_o + i\omega\xi$, with $\eta_o = [(\nabla^2\gamma)/\gamma] + (\mu_a/\gamma^2)$ and $\xi = 1/(v\gamma^2)$. For the cw case ($\omega = 0$) two sets of samples (D, μ_a) and $(\tilde{D}, \tilde{\mu}_a)$ can give rise to the same solution Ψ, if $\tilde{\eta}_o = \eta_o$ everywhere in the solution domain and $\tilde{D} = D$ everywhere within the source layer.[3]

We now derive analogous conditions, appropriate to the spectral method, wherein the parameters (D, μ_a) are replaced by (c_i, a, b). For simplicity of formulation we assume that $b(r) = b$; i.e., it is spatially constant and known. All variation in μ_s' is lumped into a, which depends on the scatterer number density and size. If multiple solutions exist for the single-wavelength measurement, then another set of functions with the same constant b and with $\tilde{a} = a + \Delta a$ and $\tilde{c}_i = c_i + \Delta c_i$ can give rise to the same measurement data. In

particular, for any arbitrary function Δa (zero within $1/\mu_s'$ of the boundary[3]), $\tilde{\eta}_o = \eta_o$ yields a condition for multiple solutions:

$$\frac{1}{h(\lambda^b, \tilde{a})} \sum_i \frac{\epsilon_i(\lambda)}{\lambda^b} \left(\frac{\Delta a}{\tilde{a}} c_i + \Delta c_i \right) = 1, \qquad (2)$$

where $h(\lambda^b, \tilde{a}) = (1/3\tilde{a})\{[\nabla^2(\lambda^b/3a)^{1/2}/(\lambda^b/3a)^{1/2}] - [\nabla^2(\lambda^b/3\tilde{a})^{1/2}/(\lambda^b/3\tilde{a})^{1/2}]\}$. Since $b(r)$ is assumed constant, $h(\lambda^b, \tilde{a})$ reduces to $h(\tilde{a}) = (1/3\tilde{a}) \times \{[\nabla^2(1/3a)^{1/2}/(1/3a)^{1/2}] - [\nabla^2(1/3\tilde{a})^{1/2}/(1/3\tilde{a})^{1/2}]\}$. Equation (2) shows that another set of functions $(\tilde{a}, \tilde{c}_i)$ produces the same boundary data for single-wavelength measurements.

For multiple wavelengths, nonuniqueness requires that Eq. (2) be satisfied for all wavelengths. Suppose there are n chromophores (c_i) and m measurement wavelengths (λ_k), then the inverse problem is not unique only if there exist solutions to the matrix equation

$$\begin{bmatrix} \frac{\epsilon_1(\lambda_1)}{\lambda_1^b} & \frac{\epsilon_2(\lambda_1)}{\lambda_1^b} & \cdots & \frac{\epsilon_n(\lambda_1)}{\lambda_1^b} \\ \vdots & & & \\ \frac{\epsilon_1(\lambda_m)}{\lambda_m^b} & \frac{\epsilon_2(\lambda_m)}{\lambda_m^b} & \cdots & \frac{\epsilon_n(\lambda_m)}{\lambda_m^b} \end{bmatrix}$$

$$\times \left(\frac{\Delta a}{\tilde{a} h(\tilde{a})} \begin{bmatrix} c_1 \\ \vdots \\ c_n \end{bmatrix} + \frac{1}{h(\tilde{a})} \begin{bmatrix} \Delta c_1 \\ \vdots \\ \Delta c_n \end{bmatrix} \right) = \begin{bmatrix} 1 \\ \vdots \\ 1 \end{bmatrix}. \quad (3)$$

We denote the wavelength-dependent matrix as $\mathbf{A}$; Eq. (3) is then $\mathbf{Ax} = \mathbf{1}$. If a solution for $\mathbf{x}$ exists, then solutions for Δc_i and $\tilde{c}_i$ that satisfy $\tilde{\eta}_o = \eta_o$ can be found.

The inverse problem has nonunique solutions if $\mathbf{Ax}$ is equal or very close to $\mathbf{1}$. With a number of wavelengths greater than the number of chromophores ($m > n$) Eq. (3) has a solution in a least-squares sense, $\mathbf{x}_o = (\mathbf{A}^T\mathbf{A})^{-1}\mathbf{A}^T\mathbf{1}$,[12] and the residual norm $R = \|\mathbf{1} - \mathbf{Ax}_o\|$ can be interpreted as the parameter distinguishability. The closer R is to zero, the closer $\mathbf{x}_o$ is to fulfilling conditions for nonuniqueness. Wavelength choices that maximize R define our first criterion for selecting optimal wavelengths.

We next consider distinguishing chromophore concentrations among themselves. The absorption coefficient for m wavelengths can be written in matrix form as $\boldsymbol{\mu}_a(\boldsymbol{\lambda}) = \boldsymbol{\epsilon}\mathbf{c}$ or

$$\begin{bmatrix} \mu_a(\lambda_1) \\ \vdots \\ \mu_a(\lambda_m) \end{bmatrix} = \begin{bmatrix} \epsilon_1(\lambda_1) & \cdots & \epsilon_n(\lambda_1) \\ \vdots & & \\ \epsilon_1(\lambda_m) & \cdots & \epsilon_n(\lambda_m) \end{bmatrix} \begin{bmatrix} c_1 \\ \vdots \\ c_n \end{bmatrix}. \quad (4)$$

The sensitivity of the measurement to a single chromophore concentration is proportional to the smoothness of the singular value distribution of the coefficient matrix $\boldsymbol{\epsilon}$ in Eq. (4). We use the condition number $\kappa(\boldsymbol{\epsilon})$ of the matrix as a measure of its smoothness, which is the ratio of the maximum to the minimum singular value. When κ is small, the singular vectors of Eq. (4) have similar contributions from each of the chromophores;

when κ is large, the measurements are much more sensitive to some chromophores than to others. Wavelength choices the minimize κ define our second criterion for selecting optimal wavelengths.

We chose different sets of four measurement wavelengths and then solved the DOT inverse problem with CW data from numerical simulations. Our samples were composed of scatterers (parameterized by a and $b = 1.3$) and three chromophores, oxyhemoglobin (HbO_2), deoxyhemoglobin (HbR), and water (H_2O). We simulated two distinct two-dimensional target media. The first medium (Fig. 2, below) had three absorption perturbations (HbO_2, HbR, H_2O) embedded in a homogeneous background; reconstructions of this medium should be most sensitive to the condition number κ, since scattering is uniform in this medium. The second medium (Fig. 3, below) had an added scattering heterogeneity. Both media had a circular geometry with a diameter of 7 cm, and each perturbation was 2 cm in diameter. The scattering parameter a and concentrations of the chromophores are listed in Table 1. Background values correspond to $\mu_a = 0.04$ cm^{-1} and $\mu_s' = 7.6$ cm^{-1} at $\lambda = 800$ nm.[7]

For both media, forward (cw) data were generated at each wavelength with 32 source and detector positions equally spaced along the circumference with a finite-element light-transport model.[13] One percent random Gaussian noise was then added to the data. DOT inversions were made with all the wavelength data simultaneously. A gradient-based optimization scheme[9] was used for reconstruction, with the unknown parameters HbO_2, HbR, H_2O, and a.

We computed R and κ for all unique combinations of four wavelength sets (Fig. 1) chosen between 650

Table 1. Chromophore Concentration and Scattering Coefficient Prefactor for Test Objects

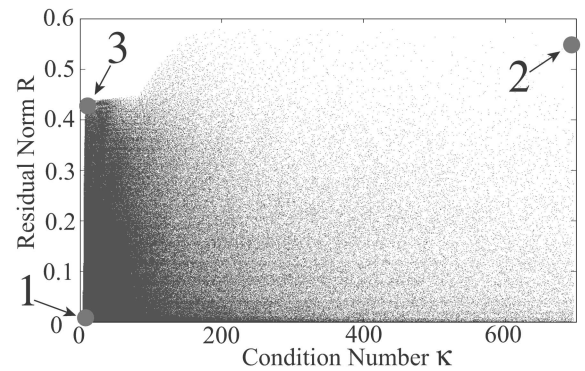|	HbO_2 (μM)	HbR (μM)	H_2O (%)	a (10^{-6b} mm^{b-1})
background	10	10	18	4500
top left	20	10	18	4500
top right	10	10	18	9000
bottom left	10	20	18	4500
bottom right	10	10	36	4500

Fig. 1. Wavelength sets with their associated residual norms, R, and condition numbers, κ. Each point represents a set of four wavelengths in the 650–930-nm range. Points 1–3 designate the sets used in the simulations.

Table 2.   Wavelength Sets and Corresponding Condition Numbers (κ) and Residual Norms (R)

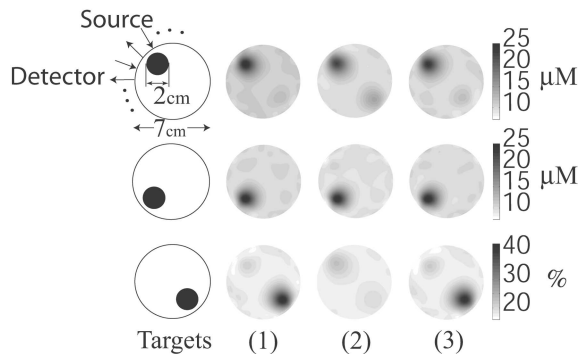| Set	Wavelengths (nm)	κ	R
1	682, 850, 854, 930	4.76	8.2×10^{-5}
2	650, 702, 714, 854	694.2	0.55
3	650, 718, 886, 930	8.29	0.44

Fig. 2.   Reconstructed images for the first target medium. The leftmost column shows images of the target objects; the top row is HbO_2, the middle row is HbR, and the bottom row is H_2O.   Columns correspond to particular wavelength sets.
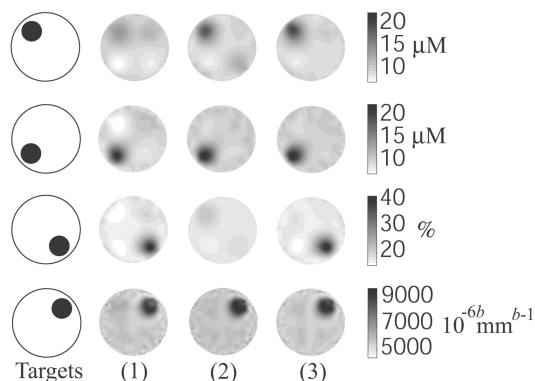

Fig. 3.   Reconstructed images for the second target medium.   Images of HbO_2, HbR, H_2O, and a are shown in the first, second, third, and fourth rows of the leftmost column, respectively.   Columns correspond to particular wavelength sets.

and 930 nm (spaced in 4-nm intervals). The extinction coefficients were taken from Ref. 14. We chose three sets of four-wavelength combinations for our reconstructions (points 1–3 in Fig. 1). These wavelength sets (see Table 2) correspond to extreme values of R and κ. Reconstruction results for the first medium are shown in Fig. 2. The three images in the leftmost column show the true locations of the target objects, HbO_2, HbR, and H_2O. The reconstructed images in subsequent columns correspond to each wavelength set. As predicted, sets 1 and 3 distinguish between HbO_2, HbR, and H_2O, but set 2 shows low contrast in the H_2O image and exhibits some cross talk between HbO_2 and H_2O. This observation demonstrates the value of our choice of κ for decoupling chromophore contributions.   Figure 3 shows the

reconstructed images for the second medium. For set 1 the addition of a scatterer caused the solution to converge to a state with a low HbO_2 contrast. Notice that the artifact in the HbO_2 image for set 1 caused by the scattering object is reduced for sets 2 and 3. These observations are consistent with our notion of maximizing R to achieve better separation of scattering from absorption.   Overall, the best contrast and separation of the four target objects were obtained with set 3; this result was anticipated because this set has high R and low κ.

Points close to point 3 provide a range of optimum wavelength sets. The wavelengths in these sets are 650 ± 2 nm, 722 ± 10 nm, 884 ± 24 nm, and 930 ± 2 nm. This range allows us a flexibility in choosing measurement wavelengths. Interestingly, the optimum wavelengths do not include values near the Hb/HbO_2 isospectic point. The first and the fourth wavelengths are at the limits of our wavelength range. However, a similar analysis without water and with sets of only three wavelengths found the last wavelength to be in the range 902 ± 16 nm. Therefore 930 nm was probably selected to distinguish water. We repeated the same analysis for a range of b from 0.8 to 1.8 and obtained similar wavelength distributions.

References

1. A. Yodh and B. Chance, Phys. Today **48**(3), 34 (1995).
2. S. R. Arridge, Inverse Prob. **15,** R41 (1999).
3. S. R. Arridge and W. R. B. Lionheart, Opt. Lett. **23,** 882 (1998).
4. Y. Xu, X. Gu, T. Khan, and H. Jiang, Appl. Opt. **41,** 5427 (2002).
5. F. Bevilacqua, A. J. Berger, A. E. Cerussi, D. Jakubowski, and B. J. Tromberg, Appl. Opt. **39,** 6498 (2000).
6. J. R. Mourant, T. Fuselier, J. Boyer, T. M. Johnson, and I. J. Bigio, Appl. Opt. **36,** 949 (1997).
7. T. Durduran, R. Choe, J. P. Culver, L. Zubkov, M. J. Holboke, J. Giammarco, B. Chance, and A. G. Yodh, Phys. Med. Biol. **47,** 2847 (2002).
8. E. M. C. Hillman, "Experimental and theoretical investigations of near infrared tomographic imaging methods and clinical applications," Ph.D. dissertation (University College London, 2002).
9. S. R. Arridge and M. Schweiger, Opt. Express **2,** 213 (1998), http://www.opticsexpress.org.
10. T. Durduran, A. G. Yodh, B. Chance, and D. A. Boas, J. Opt. Soc. Am. A **14,** 3358 (1997).
11. D. J. Durian, Opt. Lett. **23,** 1502 (1998).
12. L. N. Trefethen and D. Bau, *Numerical Linear Algebra* (Society for Industrial and Applied Mathematics, Philadelphia, Pa., 1997).
13. S. R. Arridge, M. Schweiger, M. Hiraoka, and D. T. Delpy, Med. Phys. **20,** 299 (1993).
14. S. Prahl, "Optical Properties Spectra" (Oregon Medical Laser Center, 2001), retrieved March 16, 2003, http://omlc.ogi.edu/spectra/index.html.